J. Fluid Mech. (2015), *vol.* 769, *pp.* 103–129. © Cambridge University Press 2015
doi:10.1017/jfm.2015.96

The internal wavefield generated by a towed sphere at low Froude number

A. Brandt[1,†] **and J. R. Rottier**[1]

[1]The Johns Hopkins University Applied Physics Laboratory, 11100 Johns Hopkins Road, Laurel, MD 20723-6099, USA

(Received 5 May 2014; revised 5 February 2015; accepted 8 February 2015; first published online 13 March 2015)

In highly stratified atmospheric and oceanic environments, a large fraction of energy input by various sources can be manifest as internal waves (IWs). The propagating nature of IWs results in the distribution of the energy over a large fraction of the air/water column. Wakes of translating bodies are one source of input energy that has been of continued interest. To further the understanding of wakes in strongly stratified environments, and particularly the near-field regime where strong coupling to the internal wavefield is evident, an extensive series of experiments on the internal wavefield generated by a towed sphere was performed, wherein the internal wavefield was measured over a Froude number range $0.1 \leqslant Fr \leqslant 5$ (where $Fr = U/ND$, U is the tow speed, D the sphere diameter and N the Brunt–Väisälä (BV) frequency). In a second series of experiments, the temporal wavefield evolution was studied over two BV periods. These measurements show that the body generation (lee wave) mechanism dominates at $Fr \lesssim 1$, while the random eddies in the turbulent wake become the dominant source at $Fr \gtrsim 1$. In the low-Fr regime, $Fr \leqslant 1$, there is a resonant peak in the coupling of the input wake energy to the internal wavefield at a Froude number of $\sim$0.5, and at its maximum 70 % of the input energy is coupled into IW potential energy. In this regime it was also found that the spreading angle of the evolving wavefield was considerably broader than predicted by the classical point-source models for the wavefield further downstream, owing to the existence in the near field of a significant energy content in the higher-IW modes that deteriorate at later times. In the low-Fr regime, it was found that, while the IW potential energy increases $\propto Fr^2$, the fraction of the total energy input is a weak function of Fr, varying as $Fr^{1/2}$.

Key words: internal waves, stratified turbulence, wakes

1. Introduction

Translating bodies and their wakes in stratified fluids generate internal waves (IWs) that propagate through the stratified water column. In the atmosphere, flow over mountains results in wakes and lee waves; in the ocean, wakes result from flow over seamounts and submerged bodies (Lighthill 1955; Baines 1995). These wakes, including the internal wavefield, can significantly alter the properties of the ambient

†Email address for correspondence: alan.brandt@jhuapl.edu

fluid, owing to the induced currents and turbulence resulting from wave instabilities. As a result, wakes and IWs can affect the mixing and transport of, for example, atmospheric pollutants and oceanic plankton.

1.1. *Overview of wake-generated internal waves*

Wakes in stratified fluids are inherently different from wakes in a uniform environment, not only because of the effects of stratification on the overall collapse of the vertical dimension of the wake and the suppression of vertical turbulent fluctuations, but also because of the generation of IWs that propagate away from the source and infiltrate the entire stratified water column. The internal wavefield generated by a moving body results from both body forcing (lee waves) and the random eddies in the turbulent wake (Gilreath & Brandt 1985; Dupont, Kadri & Chomaz 2001). The present study addresses the nature of the wavefield generated by a towed sphere in a continuously stratified fluid as a function of the primary governing dimensionless parameter, the internal Froude number, defined as $Fr = U/ND$, where D is the characteristic body length scale, U is the velocity, $N = (-g/\rho_0(\mathrm{d}\rho/\mathrm{d}z))^{1/2}$ is the Brunt–Väisälä (BV) or buoyancy frequency, z is the vertical distance (positive upwards), g is the gravitational acceleration, $\rho = \rho(z)$ is the depth-dependent density and ρ_0 is a reference density. The Froude number is a measure of the relative effects of inertial and buoyancy forces, and effectively defines the regimes where body forcing (at low Fr), as compared to turbulent eddy forcing (at high Fr), is the dominant mechanism for IW generation.

In actuality, the sources of IW generation are more complex than can be described simply as being due to body and wake forcing, as has been indicated by Bonneton, Chomaz & Hopfinger (1993). When a body is towed through a density-stratified environment, or alternatively when the fluid flows over a stationary obstacle (e.g. Long 1972; Chernyshenko & Castro 1996), the first (earliest in time) effect is the generation of internal waves due to fluid displacement by the body. The effective region generating IWs by body forcing also includes the recirculating zone behind the body, which, for example, extends downstream a distance of $\sim 2D$ for a circular cylinder at $Re = 2000$ and $\sim 1D$ for a sphere at $Re = 15\,000$ (Van Dyke 1982), where Re is the Reynolds number defined as $Re = UD/\nu$, with ν being the fluid kinematic viscosity. Lin, Boyer & Fernando (1992*a*) have measured the length of the recirculation zone, x_r, over a range of Fr, which for the presently considered low-Fr regime, $Fr \leqslant 1$, is constant at $x_r/D \approx 1.4$.

1.2. *Stratified wakes*

In the near-field turbulent wake behind the body (i.e. at small distances, x, behind the body), the time scale of the buoyancy force, $2\pi/N$, is greater than the elapsed time, x/U, so that the general nature of the wake appears to be similar to non-stratified wakes, exhibiting vortex-like instabilities embedded in the turbulent field at preferential Strouhal numbers (Williamson 1996). The nature of the early turbulent wake of a sphere in a stratified fluid is highly dependent on Reynolds and Froude numbers, as shown in the extensive experimental studies by Lin *et al.* (1992*a*,*b*), Chomaz *et al.* (1993*a*), Chomaz, Bonneton & Hopfinger (1993*b*), Lin, Boyer & Fernando (1994), Bonnier & Eiff (2002) and Brandt & Schemm (2011). Within the ranges of $10 \leqslant Re \leqslant 10^4$ and $0.01 \leqslant Fr \leqslant 20$, three regimes have been identified by Lin *et al.* (1992*b*): symmetric vortex shedding at low Re and Fr; non-symmetric vortex shedding at intermediate Re and Fr; and fully turbulent (no clear coherent vortices) at high Re and Fr. Chomaz *et al.* (1992) have also shown

the dependence of the flow separation line on Froude number and the presence of a resonance for generating lee waves at $Fr = 0.5$.

Even at less than one buoyancy period, $2\pi/N$, the effects of stratification are evident. At $Nt \sim 1$, where t is the time after passage of the body, generally measured from the sphere centre, the vertical extent of the wake reaches a maximum (Lin & Pao 1979; Gilreath & Brandt 1985). From that time on, the mean wake height first decreases and then oscillates about its final level, while the wake width increases in a manner similar to the collapse of an impulsive turbulent patch (Wu 1969; DeSilva & Fernando 1998). In this regime, however, the wake velocity defect and turbulence level decrease in a manner surprisingly similar to unstratified decay (Spedding, Browand & Fincham 1996*a*,*b*; Spedding 1997). Further downstream, the wake enters a non-equilibrium regime at $Nt \approx 2$, with a decreased decay rate until $Nt \approx 50$, when the decay rate increases again and the wake is in a quasi-two-dimensional state with the formation of late-wake 'pancake' eddies (Lin & Pao 1979; Spedding 1997). This evolution is the result of entrainment, residual instabilities from the early wake and energy redistribution in the vertical. As the wake evolves, it begins to undulate in the horizontal plane, leading to the formation of late-wake eddies that persist for long times and organize into dipole structures (Brandt 1999). It is of interest to note that, while these structures have an appearance similar to the von Kármán vortices in low-*Re* laminar wakes (Williamson 1996), the generation mechanisms are quite distinct. Late-wake evolution is the subject of extensive studies by Spedding and colleagues (Spedding *et al.* 1996*a*,*b*; Spedding 1997), and are not further explored in the present report. A recent review by Spedding (2014) provides an overview of the self-similar evolution of stratified wakes.

1.3. *Body and turbulent wake-generated internal waves*

At early times, the displacement of the fluid by the moving body will generate IWs. Body-forced lee waves are present in all situations but tend to be the dominant IW source at low *Fr*. At higher *Fr*, turbulent wake-generated IWs dominate (Dupont *et al.* 2001). In this regime, the turbulent eddies within the wake will result in the generation of IWs. Although the extent of the collapse of the mean wake is relatively small, for a propeller-driven body the stratified wake is well mixed, so that the wake collapse is a significant mechanism for generating IWs (Lin & Pao 1979; Gilreath & Brandt 1985). For a towed sphere, the degree of mixing is substantially less, so that the global collapse of the wake does not contribute substantially to the generation of IWs, as discussed by Bonneton *et al.* (1993). The transition between the lee wave IW regime and the turbulent-wake-generated random wave regime has been found to occur at $Fr = 2$ by Chomaz *et al.* (1991), Hopfinger *et al.* (1991), Lin, Boyer & Fernando (1993) and Robey (1997). However, the transition between regimes is not precise, as there is a range of *Fr* where both mechanisms can generate IWs. In the present study utilizing a towed sphere, the existence of a random wavefield component at low Froude numbers and at early times is also evident.

In the lee wave regime, Chomaz *et al.* (1993*b*) found that the amplitude of the IW initially grows $\propto Fr$ and reaches a maximum at $Fr = 0.5$–0.7. Robey (1997), using a layered stratification, found an amplitude maximum occurring at $Fr = 0.7$–0.8. This range corresponds to the location of the peak in the drag coefficient in the vicinity of $Fr = 0.5$–0.8 measured by Lofquist & Purtell (1984), indicating the strong coupling between the body and the IW field in this range. Similar results are presented in the present study in terms of the IW potential energy (PE).

There has been extensive modelling of the lee wavefield generated by towed sources, starting with kinematical descriptions, generally using point and spherical sources (e.g. Keller & Munk 1970; Sharman & Wurtele 1983; Voisin 1994; Dupont & Voisin 1996; Lighthill 1996; Scase & Dalziel 2004, 2006; Voisin 2007). The latter papers extend the analyses using dynamical models to predict wave amplitudes and wave drag as functions of Fr, with excellent agreement with experiments. Also relevant are the related studies of lee wave flows over topographic obstacles (i.e. objects mounted on a fixed surface) (Castro, Snyder & Baines 1990; Vosper *et al.* 1999; Dupont *et al.* 2001; Dalziel *et al.* 2011). Although many of these studies are at low Re, they exhibit the same wavefield features as objects towed in an unbounded flow. Of particular interest is Castro *et al.* (1990), where the effect of tank depth is shown to have a significant effect on the object drag, decreased values corresponding to integral values of $K = NH/\pi U$ (essentially the inverse of a Froude number based on the tank depth H). Voisin (2007) has extensively reviewed the analytical IW theories and determined the IW structure for the high- and low-Fr regimes, as well as modelling the wave drag component. The recent work of Vasholz (2002, 2011) using a Green function approach shows the existence of a broad resonance due to the effects of stratification, as well as multiple resonances (i.e. peak values) of the IW PE at select values of Fr due to the effects of the rigid-lid boundary conditions. In the limit of infinite depth, only buoyancy-induced resonances are present at low values of Fr, the maximum of which for a sphere occurs at $Fr \sim 0.46$. It should be noted that analytic models of the internal wavefield (Sharman & Wurtele 1983; Vasholz 2002, 2011; Voisin 2007) are formulated in terms of Fourier modes whose superposition (which would correspond to experimentally measured waveforms) does not generally produce smoothly defined waveforms (see particularly Sharman & Wurtele 1983). At low Fr, below the mode-dependent critical values (Vasholz 2011), the coupling of the body-forced IW is significantly stronger than at higher Fr, as evidenced by the increase in drag (Lofquist & Purtell 1984; Greenslade 2000; Voisin 2007), and the wavefield includes transverse as well as divergent waves (Sharman & Wurtele 1983; Robey 1997; Vasholz 2011). The peak in the increase in drag at $Fr \simeq 0.5$ (Lofquist & Purtell 1984; Chomaz *et al.* 1993*b*; Greenslade 2000; Voisin 2007) corresponds to the buoyancy-induced resonance in the internal wavefield (Sharman & Wurtele 1983; Vasholz 2002, 2011; Voisin 2007). In a tank of finite depth, multiple IW resonances are present at specific values of a depth-based Froude number $Fr_H = U/NH$ (Castro *et al.* 1990; Vosper *et al.* 1999; Vasholz 2002). These finite-depth resonances occur at specific values at each mode n, according to $Fr_H = 1/n\pi$. There is, however, a seeming contradiction at these integer values of Fr_H: Castro *et al.* (1990) and Vosper *et al.* (1999) find a drag minimum, while the analysis of Vasholz (2002) predicts an IW PE maximum. It is a possibility that the behaviour of drag variations measured by Castro *et al.* (1990) and Vosper *et al.* (1999) at $Fr \gtrsim 1$ is different from the model of Vasholz (2002) and the present experiments, where the resonances were observed in the $Fr \leqslant 1$ regime; or that the former relates to the drag due to downstream lee waves, upstream columnar vortices and wake-generated IWs, while the latter relates to lee wave PE, which again may have different behaviours.

Random IW generation results from the motion of the large-scale coherent structures in the turbulent wake, as was initially observed using a self-propelled body by Lin & Pao (1979) and was first experimentally demonstrated in Gilreath & Brandt (1985). While random IWs are a significant contributor to the IW field at high Fr (Gilreath & Brandt 1985), it was found that both the lee waves and random waves contributed to the resultant IW field. The link between coherent structures in the wake of a sphere

and the random IW was shown by Lin *et al.* (1993), Bonneton *et al.* (1993, 1996) and Robey (1997). In particular, Bonneton *et al.* (1993) have shown the presence of random IWs due to the initial wake impulse and to the later-time coherent structures, with amplitudes that both increase proportionally to Fr^2 and decay as $(Nt)^{-1}$. Robey's (1997) experiments used a mid-depth thermocline stratification (as opposed to the other cited studies, which used a linear stratification) and found random IW amplitudes increasing with Froude number at a rate significantly less than Fr^2. Internal waves will inherently fill the entire stratified water column. In these experiments (Robey 1997), only a thin region of the water column was stratified so that the IW field was confined to that pycnocline region. This will inevitably affect the coupling of the lee wave and turbulent wake to the IW field, as evident in the depth dependence in the analytic expressions derived by Vasholz (2002, 2011).

In any experimental realization, wake-turbulence-generated IWs will, to some degree, arise from random turbulent eddy structures within the wake (Gilreath & Brandt 1985; Bonneton *et al.* 1993; Robey 1997). The separation of the propagating IW components and the late-wake residual vortical modes has been addressed by Lelong & Riley (1991), Riley, Lelong & Slinn (1991) and Lighthill (1996). These studies clarify the mechanisms responsible for the energy redistribution; however, the exact nature of IW generation by wake turbulence remains speculative.

Models for the turbulence-generated IW field have been considerably less numerous. Gilreath & Brandt (1985) presented an estimate for the vertical propagation of the random wavefield in terms of the angle from the horizontal, θ_c, based on the observed frequency of the measured wake eddy frequency, ω_0, as

$$\theta_c = \tan^{-1}\left[0.4\left(\frac{\omega_0}{N}\right)^{-1}\right], \tag{1.1}$$

which agreed with the wavefield measurements for the self-propelled slender body. Robey (1997) used the wake eddy properties to initialize a numerical model, which provided good agreement with the growth of wave amplitude generated by a towed sphere in the random wave regime. Voisin (1995) developed a model based on the vortex shedding in the wake as

$$\theta_c = \frac{2}{3^{3/2}\Upsilon} \approx \frac{0.385}{\Upsilon}, \tag{1.2a}$$

with

$$\Upsilon = \frac{\omega_0}{N} = 2\pi Fr\, St \tag{1.2b}$$

where $St = fD/U$ is the Strouhal number and $f = \omega_0/2\pi$ is the oscillation frequency. This agrees almost exactly with (1.1) and the experimental data in Gilreath & Brandt (1985) using $St \simeq 1$ as appropriate for a slender body.

At low Fr, say $Fr = 2$, as relevant to the present study, a sphere with $St \simeq 0.2$ yields $\theta_c = 8.6°$ via (1.2), as compared to 0.44° for the high $Fr \simeq 8$ slender body in Gilreath & Brandt (1985). This implies that, for a turbulent sphere wake at $Fr = 2$, random waves would appear one diameter above the body as early as $x/D = 6.5$ (or ∼0.5 BV periods), and even closer for smaller values of Fr.

Numerical simulations of stratified wakes have generally focused on the turbulent wake region itself (e.g. Gourlay *et al.* 2001; Brucker & Sarkar 2010; Diamessis, Spedding & Domaradzki 2011) and on the turbulent wake-generated internal wavefield (e.g. Meng & Rottman 1987; Rottman *et al.* 2006; Diamessis, Gurka &

Liberzon 2010; Diamessis *et al.* 2011; Abdilghanie & Diamessis 2013), using smooth self-similar initial velocity and density profiles at a short distance downstream of the body. As a result, the IW simulations represent the contributions due to the turbulent wake, essentially the high-Fr case, and reproduce reasonably well the wavefield characteristics. Of note in the present context is the dependence of the vertical opening angle of the horizontal vorticity on the proper orthogonal decomposition (POD) mode shown by Diamessis *et al.* (2010) and the decrease in the horizontal IW wavelength with Nt. In contrast to these numerical turbulent wake-generated IW studies, Chang *et al.* (2006) utilized a Reynolds-averaged Navier–Stokes (RANS) simulation of the flow around a submerged body as the initial conditions for calculating the IW field in a two-layer fluid at subcritical Fr, thus simulating the lee wave generation process with good agreement with the analytical model of Sharman & Wurtele (1983).

1.4. *Focus of current effort*

The present study focuses on experimental measurements of the generation of IWs at early times at low Froude numbers in a constant-N environment, wherein body forcing is the dominant IW generation mechanism. This expands on the experiments of Robey (1997), where horizontal internal wavefield measurements were made in a thin thermocline layer, and on the other studies cited above that were generally limited to IW measurements at specific points. The present measurements cover a significant portion of the vertical plane, allowing for the characterization of the IW dispersion and propagation as a function of Fr and distance downstream. The IW PE is examined in order to demonstrate and quantify the strong coupling to the IW field at low Fr. The existence of a non-negligible random IW component at low Fr is also demonstrated. The following section describes the experimental methodology. Section 3 presents the experimental results including properties of the turbulent wake, evolution of the mean IW field, characterization of the random IW, and the variation of the IW PE as a function of Fr and distance downstream. Section 4 provides a discussion and summary.

2. Experimental approach

2.1. *Apparatus and experimental conditions*

The experiments were conducted in the Johns Hopkins University Applied Physics Laboratory stratified towing tank facility. The tank is 7.6 m $\times$ 1.8 m $\times$ 0.8 m deep (figure 1) and is stratified by introducing layers of increasingly saline water through a slotted header that extends along the full length of the tank bottom. The tank and experimental procedures are similar to those used in the earlier experiments on IWs (Gilreath & Brandt 1985). For the present experiments, the tank was stratified to a depth of 0.59 m, with a 6 cm fresh water layer overlying a linearly stratified region extending to the tank bottom, schematically illustrated in figure 1. This configuration was selected in order to have the IW probe rake (see § 2.2) encompass the majority of the fully stratified region above the sphere model. The tank stratification was attained using a filling system that draws fresh and saline water from storage tanks in accordance with a preprogrammed schedule corresponding to the desired BV frequency. Specifically, as the fluid rises, the water depth is monitored by a capacitance wire circuit, the desired density computed from the input density gradient profile, $N(z)$, and signals sent to control the speeds of the fresh and saline water pumps. (The densities in the storage tanks are monitored using real-time temperature

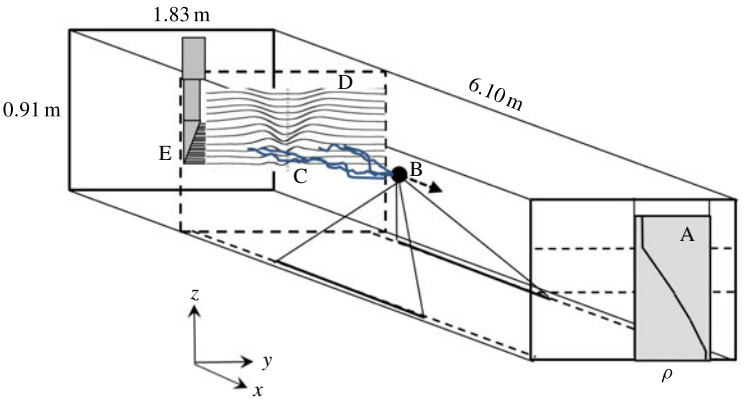

FIGURE 1. (Colour online) Schematic of stratified tow tank: A, density profile; B, towed sphere; C, turbulent wake; D, internal wavefield; E, conductivity probe rake.

and salinity gauges.) Anomalies in the density profile smooth out over several hours (typically overnight), giving a uniform gradient. The tank filling and all other measurements described below were controlled by a LabView® virtual instrument (VI), on a PC equipped with analogue–digital and digital–analogue input–output interfaces.

Measurements of the ambient tank stratification profile are made using vertically traversing conductivity and temperature probes, at a speed of $\sim$1 cm s^{-1}. The conductivity probe is calibrated using solutions of known salinity and temperature. Upward- and downward-moving profiles are averaged to eliminate small differences due to probe lag. For the present experiments, a uniform stratification was used, with a nominal BV frequency of 1.20 s^{-1} (5.2 s period) for the majority of the experiments, and a standard deviation over the test depth range of $<$0.05 s^{-1} for a given tank stratification. To achieve higher values of Fr, additional runs were made with $N = 0.20$ s^{-1}. Towing the model during an experimental run disturbs the ambient stratification, which recovers very slowly. After several runs (typically four to six depending on the model tow speed), there is sufficient distortion to the density profile (i.e. $>10\,\%$) that the tank has to be restratified.

A sphere of diameter 9.50 cm located at a depth of 27.5 cm below the surface was used in all experiments. The sphere was buoyant and supported by crossed fine wires (0.013 cm in diameter) attached to sliding tubes on towing cables at the tank bottom that were pulled at a controlled speed by a motor-driven towing system (see figure 1). At the maximum tow speed, nominally 25 cm s^{-1} or less, the Reynolds number based on the wire diameter is less than 32, so that the effects of the support wires on the wake flow field are negligible, as was apparent from direct observations during the experiments. The surface of the sphere was roughened by gluing sand grains on the surface in order to ensure a stable turbulent transition.

The model speed range employed was $U = \{1.1, 24\}$ cm s^{-1}, giving a range of $Fr = \{0.09, 5.03\}$ and $Re = \{1083, 22\,400\}$. The Froude number ranges from the clearly lee wave regime to the point where random waves become significant. Here, Re values encompass marginally turbulent values to values with clearly turbulent wakes. Model oscillations on the supporting wires were found to be negligible in measurements of the spectral response of sphere motion using sequential video images, made in conjunction with other related studies. The model was started from a rest position,

accelerated to its final speed over a distance of ∼0.5 m, towed at the desired speed through the test section (where the probe rake traversed the wake, § 2.2 below), and stopped ∼2.5 m upstream of the test section, which was sufficiently far to avoid contamination by the stopping transient. The speed of the sphere was measured using a linear shaft encoder monitored by a LabView VI.

2.2. *Internal wave probe rake*

Since the tank is stratified by varying the salinity as a function of depth, the specific conductance of the ambient fluid is a function of depth. This circumstance allows vertical displacement to be measured with a single-electrode conductivity probe (using an AC bridge circuit grounded with a nickel strip in the bottom of the tank) that responds to conductance changes in the immediate vicinity of the small (0.025 mm) platinized electrode at the tip of the probe. A vertical array of 19 conductivity probes spaced at nominal 1 cm intervals was used. The rake traversed the tank at a specified distance behind the sphere to map out the cross-plane IW field. The lowermost probe was positioned at the sphere centreline so that the measured IW field spanned an 18 cm region above the model centreline, covering 86 % of the stratified upper half of the tank water column. This is sufficient to characterize the evolving wavefield assuming a symmetric wavefield above and below the model. Extrapolations to the upper stratified region are used for estimating the IW PE, as discussed in § 3.4.

The probes were calibrated by displacing the entire rake at multiple 0.5 cm intervals above and below the rest position, thus giving an (almost linear) calibration for each probe in terms of voltage versus depth. When the probe rake traversed the wake, the fluid displacements were then registered as conductivity changes. The resulting resolution of the wave amplitudes is estimated to be <0.1 mm.

A high-speed pneumatically driven carriage was used to literally 'fire' the probe array across the test section to obtain a snapshot of the wavefield at a selected distance aft of the sphere. The path of the probe was adjusted to an angle that corresponds to the relative speed of the sphere and the probe motion, in order to have the cross-track data correspond to a fixed downstream distance. The nominal speed of the probe carriage was 1.5 m s^{-1}. Data were digitized at 250 Hz so that the nominal spacing of the data points corresponded to 0.6 cm, which is adequate for resolving the internal waves, whose typical wavelength range is ∼10–30 cm. An example of the cross-track IW fields for three repeat runs at the same values of Fr, Re and distance downstream, Nt, is shown in figure 2. Additional post-collection corrections for the IW field were made by adjusting the overall wave amplitudes to correspond to slight, O(mm), errors in the height of the cross-tank probe array strut, using the ends of the cross-track data where the IWs have not as yet affected the ambient fluid levels as well as calibration runs with no model-induced disturbances. The speed and location of the probe rake was measured using photodetector indicators at two fixed cross-track positions.

3. Results

3.1. *Description of IW data and scope of experiments*

As mentioned, figure 2 shows three cross-track IW repeat runs. The towed sphere was centred at $y = 0$, $z = 0$, so that its vertical extent is $D/2 = 4.25$ cm. Near the sphere depth, $z = 0$ to ∼4 cm, the presence of the turbulent wake is evident. These data are aliased, as the data acquisition rate, sufficient to capture the IW field, was inadequate to capture the turbulent fluctuations (further studies on the wake density fluctuations

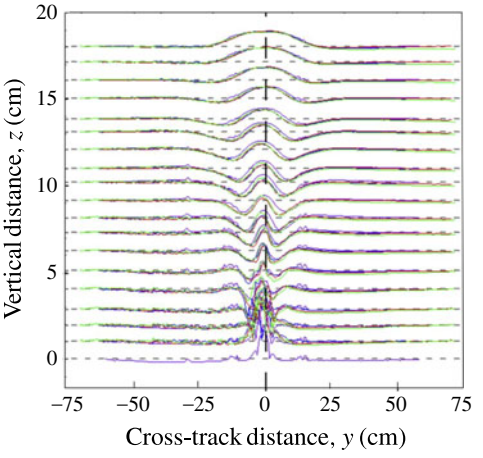

FIGURE 2. (Colour online) Three repeat internal wavefield measurements at $Fr = 1/\pi$, $Nt = 2\pi$ $(x/D = 2.0)$. The towed sphere is centred at $y = z = 0$. Dashed lines are probe locations. Wavefield displacements are to the same scale.

have been performed and have been reported by Brandt & Schemm (2011)). Above this region, the vertical structure of the IW field is evident. (The wave amplitudes are plotted on the same scale as the vertical axis, showing the probe depth positions.) The lack of exact repeatability of the IW field is attributed to the random wave contributions and to some degree of experimental error. Differences between repeat runs are less pronounced with increasing height above the wake in accordance with the expectation that the random IWs would have shorter wavelengths and thus slower vertical propagation speeds than the lee waves, as discussed in Gilreath & Brandt (1985). The residual differences between repeat runs outside the turbulent wake region are likely to be due to the contribution of the recirculating near-wake region behind the sphere, which is inherently not exactly repeatable, as well as minor differences in the ambient stratification between runs.

An extensive series of experiments has been performed to explore the evolution of the IW field in the low-Froude-number early-wake regime. As discussed above, the stratification was maintained constant so that the values of Fr and Re were determined solely by the model speed. The scope of the run combinations exploring the effects of Froude number at $Nt = 2\pi$ is shown in table 1. The number of repeat runs, n, at each condition is also shown. For a limited number of runs, a weaker stratification was used, $N = 0.20$ s^{-1}, as shown in the bottom rows in table 1. At $N = 0.20$ s^{-1}, a value of $Fr = 5$ was attained. Higher values of Fr could not be attained, because, at higher speeds in the weak stratification, the turbulent wake was significantly larger, encompassing a large portion of the probe rake, thus invalidating the IW measurements. The individual runs were grouped in narrow bins representative of each value of Fr. Shown in table 1 are the standard deviations of the run parameters for each run group; the low values justify the nominally identical conditions within each run group.

While the present experimental effort was focused on examination of Froude-number variations, the effect of the corresponding Reynolds-number variations is of potential concern. The experiments were performed within a Reynolds-number regime where the unstratified drag on the sphere is essentially constant (Schlichting

Fr	n	U (cm s^{-1})	N (s^{-1})	σ_{Fr}	Nt	σ_{Nt}	Re	σ_{Re}
0.09	5	1.1	1.20	0.01	6.18	0.42	1 083	68
0.13	3	1.6	1.20	0.01	5.69	0.85	1 492	138
0.16	3	1.9	1.20	0.01	6.53	5.65	1 843	155
0.18	2	2.2	1.20	0.01	4.63	1.18	2 071	107
0.19	3	2.4	1.20	0.01	6.55	0.27	2 286	111
0.22	3	2.7	1.20	0.01	6.41	0.05	2 521	113
0.28	1	3.3	1.20	—	6.35	—	3 088	—
0.31	10	3.7	1.20	0.02	6.42	0.10	3 528	183
0.36	3	4.3	1.20	0.00	6.68	0.75	4 050	54
0.44	3	5.3	1.20	0.02	6.49	0.06	5 022	287
0.53	2	6.4	1.20	0.03	6.19	0.05	6 113	316
0.98	4	11.9	1.20	0.03	6.30	0.07	11 279	440
1.95	3	23.2	1.20	0.02	6.26	0.00	22 040	272
1.91	3	4.3	0.20	0.07	6.36	0.459	4 107	70
5.03	5	11.1	0.20	0.07	6.26	0.050	10 545	503

TABLE 1. Run conditions for Froude-number variation experiments at $Nt = 2\pi$ ($N_c t = 1.0$).

1968), so that the effects of the stratified background on the sphere drag can be clearly identified with Froude-number effects, as shown by Lofquist & Purtell (1984) and Greenslade (2000). It can therefore be inferred that the nature of the internal wavefield is dominated by stratification, i.e. Froude-number variations rather than Reynolds-number effects. Moreover, at the one condition where N was varied, $Fr \approx 2$, and the Reynolds numbers were 4.1×10^3 and 22.0×10^3, the computed IW PE shown in figure 10 had essentially the same values, further implying the dominance of Froude-number effects on the nature of the IW field.

A series of runs was also made to explore the temporal (or downstream) evolution of the IW field. At each combination of Fr and Nt values, a number of runs were made (typically three to five for the Fr variation study, and four to 10 for the Nt variation study) to ensure repeatability and to explore the contribution of the random IWs. Table 2 presents a listing of the runs exploring variations in Nt at $Fr = 1/\pi \approx 0.32$. The downstream locations were selected to have roughly equal spacing in terms of the number of BV cycles, i.e. nominal values of $N_c t = \{1.0, 1.5, 2.0, 2.5, 3.0\}$, where $N_c = N/2\pi$, with the time and downstream distance measured from the sphere centre. (Correspondingly the cyclic Froude number, $Fr_c = 2\pi Fr$, for these runs was $Fr_c = 2.0$. For the Froude-number variation study, $Fr_c = \{0.60, 12.2\}$.) For the range of test conditions, $Re = \{1.1, 22.0\} \times 10^3$. As the primary experimental variable was the towing speed of the sphere, the variations in Fr were accompanied by changes in Re. In the Re range employed, Re is sufficiently large to be within the turbulent regime where the nominal, unstratified, drag coefficient is essentially constant (Schlichting 1968), implying that, for the stratified flows considered herein, the generation of body-generated IWs is primarily a function of the Froude number, while the turbulent wake and the associated wake-generated IWs can be characterized in terms of both Fr and Re.

3.2. *Mean wavefield*

3.2.1. *Experimental results*

Figure 3 presents four independent realizations and their mean of the cross-track IW fields at $Fr = 1/\pi$, $Nt = 15.3$. These data are at the same Froude number as the IWs

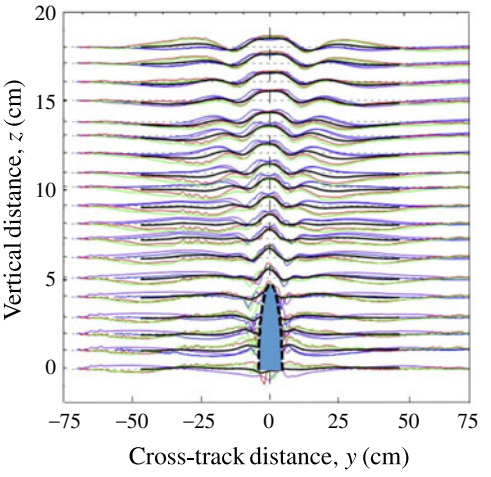

FIGURE 3. (Colour online) Four repeat internal wavefield measurements (thin lines) and their mean (thick line) at $Fr = 1/\pi$, $Nt = 15.3$ $(x/D = 4.9)$. The towed sphere is centred at $y = z = 0$ and shown as a shaded region. Dashed lines are probe locations. Wavefield displacements are to the same scale.

$N_c t$	Nt	n	σ_{Nt}	Fr	σ_{Fr}	Re	σ_{Re}
1.02	6.42	10	0.10	0.31	0.02	3528	183
1.21	7.59	4	0.05	0.32	0.01	3603	120
1.43	9.01	5	0.17	0.33	0.01	3637	49
1.57	9.86	4	0.39	0.32	0.01	3653	173
2.03	12.77	6	0.14	0.31	0.01	3542	147
2.43	15.29	6	0.81	0.32	0.01	3566	107
3.03	19.06	5	0.16	0.31	0.01	3545	133

TABLE 2. Run conditions for downstream variation experiments at $Fr = 1/\pi$ $(Fr_c = 2.0)$.

shown in figure 2, but at a later time/downstream distance ($x/D = FNt = 4.9$ compared to $x/D = 2.0$ in figure 2). In figure 3, the evolution of the wavefield at 2.5 cycles ($N_c t = 2.43$) is manifested in terms of two waves on each side of the centreline resulting from the continuous forcing by the sphere and its attached recirculating region, as compared to the single symmetric wave evident in figure 2. The mean of the four wavefield realizations reduces the effects of the turbulent wake-generated IWs and the variability due to forcing by the near-wake recirculating region, and provides a characterization of the body forcing component of the IW field. The run-to-run variability of the IW field is the result of the unsteady recirculation zone behind the sphere and the random turbulent wake generated IWs. It also should be kept in mind that towed sphere IWs result from a translating source, significantly different from continuous forcing by, for example, a vertically oscillating cylinder (e.g. Mowbray & Rarity 1967). The mean IW fields for each group of runs, listed in tables 1 and 2, are used to characterize the Fr and Nt dependences.

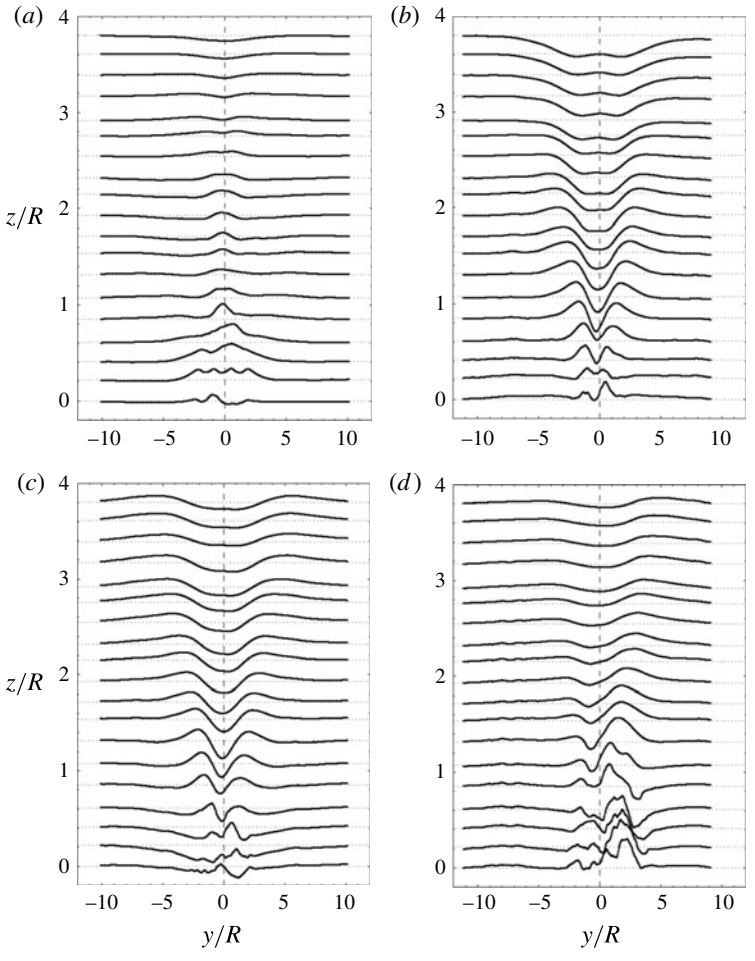

FIGURE 4. Froude-number dependence of mean internal wavefield, $Nt = 2\pi$: (*a*) $Fr = 1/(2\pi)$ $(x/D = 1.0)$; (*b*) $Fr = 1/2$ $(x/D = \pi)$; (*c*) $Fr = 1$ $(x/D = 2\pi)$; (*d*) $Fr = 2$ $(x/D = 4\pi)$.

3.2.2. *Froude-number effects*

The mean IW fields for four series of runs is shown in figure 4 in dimensionless coordinates scaled by the sphere radius, R, illustrating the nature of the internal wavefield at different Froude numbers at one BV period, $Nt = 2\pi$. (It should be noted that, at a fixed value of x/D, rather than a fixed value of Nt, as shown in figure 4, the variation of the internal wavefield pattern would be dominated by the number of BV cycles elapsed as $Nt = (x/D)/Fr$, much like the patterns shown in figure 5.) In these plots, IW forcing due to the body generation is evident by the uniformity of the wavefield at lower Froude numbers (figure 4*a*,*b*) and at larger distances above the sphere wake. In contrast, wavefield distortions and asymmetries resulting from wake-generated IWs are present close to the sphere ($z/R \lesssim 1$) and are considerably stronger at the higher-Fr, higher-Re conditions (figure 4*c*,*d*). The presence of random wake-generated IWs at these early times is in agreement with the calculations based on (1.2) discussed above; for example, at $Fr = 2$ (figure 4*d*), random IWs would be present at $Nt \sim \pi$, well before the time of these IW measurements. The asymmetry in

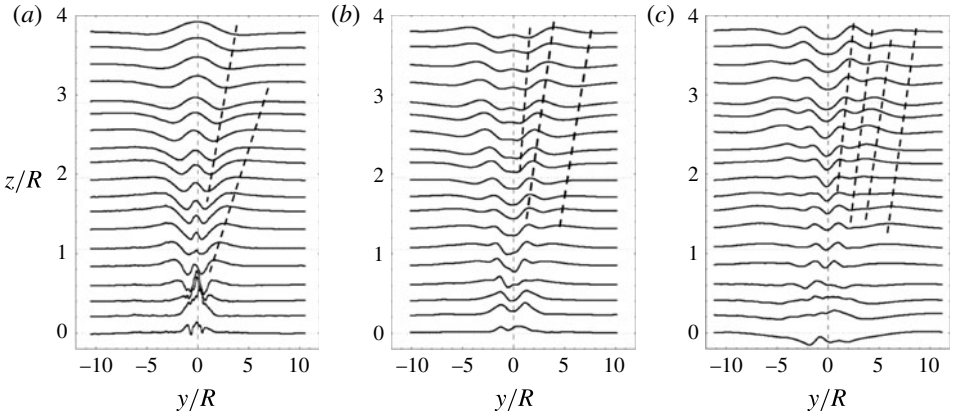

FIGURE 5. Temporal evolution of mean internal wavefield, $Fr = 1/\pi$: (*a*) $N_c t = 1$ $(x/D = 2.0)$; (*b*) $N_c t = 2$ $(x/D = 4.0)$; (*c*) $N_c t = 3$ $(x/D = 6.0)$.

the internal wavefield evident at the higher Fr (and Re) values shown in figure 4(*d*) is due to the fact that, at these high values, the random wake turbulence is the dominant contributor to the internal wavefield. As a result, the number of ensemble runs averaged is not sufficient to provide an accurate mean wavefield. The integrated internal wavefield PE, however, has considerably less variability as discussed in § 3.4.2.

Qualitatively, the amplitudes of the IWs in the region above the turbulent wake $z/R \gtrsim 1$ appear to be larger at the intermediate Froude numbers (figure 4*b*,*c*). This is indicative of a stronger coupling of the body source to the IW field at specific values of Froude number, as found in earlier studies, and will be further discussed in § 3.4. Since the limited ensemble used to estimate the mean internal wavefield as shown in figure 4 does entirely remove the random waves, the region of their influence is considered. The spread of wavefronts in the random IW field can be computed from the expressions given by Voisin (1994) for a translating oscillating dipole at arbitrary values of Υ in the parametric form

$$(y, z) = x \tan\theta_{\pm}\left(\frac{|\sin\phi|}{\Upsilon}\right)(\cos, \sin)\phi, \tag{3.1}$$

where ϕ is the azimuthal angle and $\theta_{\pm}(|\sin\phi|/\Upsilon)$ is the polar angle. For the present experiments, (1.2*b*), $\Upsilon = \{0.1, 6.3\}$, it can be shown that, when the wavefield is decomposed into sum and difference components, the wavefronts become increasingly confined to a narrow band around the $y = 0$ axis (Voisin 1994). This agrees with the observed asymmetry in figure 4(*d*) that is confined to $y/R \lesssim \pm 3$. The strength of the random IW field is dependent on the strength and scales of the coherent eddies in the turbulent wake, which are functions of Re and Fr, and how they are related to the dipole source in this model.

3.2.3. *IW propagation in the vertical plane*

The temporal evolution of the mean IW field at $Fr = 0.32$ over three successive BV periods, $N_c t = \{1.0, 2.0, 3.0\}$, is shown in figure 5. The effective body forcing due to the body itself and the near-field recirculating wake, the latter of which is not as

effective as the body in displacing the surrounding fluid, generates the IW field with an increasing number of waves, corresponding roughly to the number of elapsed BV periods. In addition to the strong wavefield displacement directly above the sphere that was evident in the slender-body experiments in Gilreath & Brandt (1985), the angle, θ, of the IW beams with the vertical and the propagation of the IWs are evident in the present data. The wave beam angle is related to the effective forcing frequency, ω, by the linear dispersion relationship (Mowbray & Rarity 1967)

$$\frac{\omega}{N} = \cos\theta, \tag{3.2}$$

where θ is the angle between the wave group speed and the vertical. The present IW data are cross-track vertical plane cuts through the wave beams, so that a line through successive wave crests (and troughs) along the beam corresponds to the direction of the IW group velocity, c_g. It is recognized that the actual structure of the wavefield is such that wave rays emanating from the sphere have varying frequency and inclinations, as illustrated in Voisin (1994, 2007) and Vasholz (2011) and particularly in the combined mode plots in Sharman & Wurtele (1983) and the cross-plane cuts illustrated in Sturova (1978, 1980). Nevertheless, the experimental cross-plane cuts show an apparent dominant wave pattern, which is used to qualitatively characterize the wavefield, as has been employed in other experimental investigations (e.g. Cerasoli 1978; Dohan & Sutherland 2005). This wavefield characterization approach also pertains to the cuts in the horizontal plane discussed in § 3.2.4.

To estimate θ, the angles of the crest and trough of the first wave (farthest off track) and the crest of the second wave were measured. These were readily tracked through the sequence of conditions listed in table 2, as illustrated by the dashed lines in figure 5. The evolution of the measured angles is shown in figure 6(*a*) in terms of ω/N according to (3.2), with an average $\omega/N \simeq 0.5$, $\theta \simeq 60^\circ$ and a spread corresponding to $\theta \simeq 55^\circ$–65°. The estimated measurement error is $\sim$10 % for these data, as well as for the wavelength values shown in figure 6(*b*). These values of θ are somewhat larger than the range measured by Dohan & Sutherland (2005), $\theta = 46 \pm 5^\circ$, for IWs generated by a continuous turbulent source, by Cerasoli (1978) for IWs resulting from the collapse of a buoyant plume where the angle ranged between $\theta = 35^\circ$ and 50°, and by Wu (1969) for the collapse of a mixed region where $\theta = 36^\circ$. In numerical simulations of wake turbulence, steeper angles were found by Diamessis & Abdilghanie (2011), with $\theta = 31^\circ$ at low $Re = 5 \times 10^3$ and $\theta = 45^\circ$ at the higher $Re = 10^5$. These lower angles are not unreasonable since the turbulent wake-generated IWs have shorter wavelengths and higher frequencies than the body displacement IWs. Dohan & Sutherland (2005) have used linear theory to estimate the angle at which the waves carry the maximum vertical flux away from a turbulent source as 45° ($\omega/N = 0.7$). Deviations of the experimental data from this value could be due to experimental error and/or nonlinear interaction effects.

Wavelengths associated with the mean IW field were estimated from the temporal evolution data represented by figure 5. Figure 6(*b*) shows the IW wavelengths, λ, measured at three elevations above the turbulent region where the body-generated IWs clearly dominate, using peak-to-trough values of the clearly dominant wave. While these data are limited, the increase in λ/D with distance from the source and with increasing values of Nt is apparent. (Chomaz *et al.* (1993*b*) found that the horizontal along-track wavelength (as opposed to the cross-track measurements obtained herein) was strongly Fr-dependent, with a value of $\lambda/D \simeq 8$ at $Fr = 0.32$.) The present values of λ/D are considerably greater than the wavelengths computed by

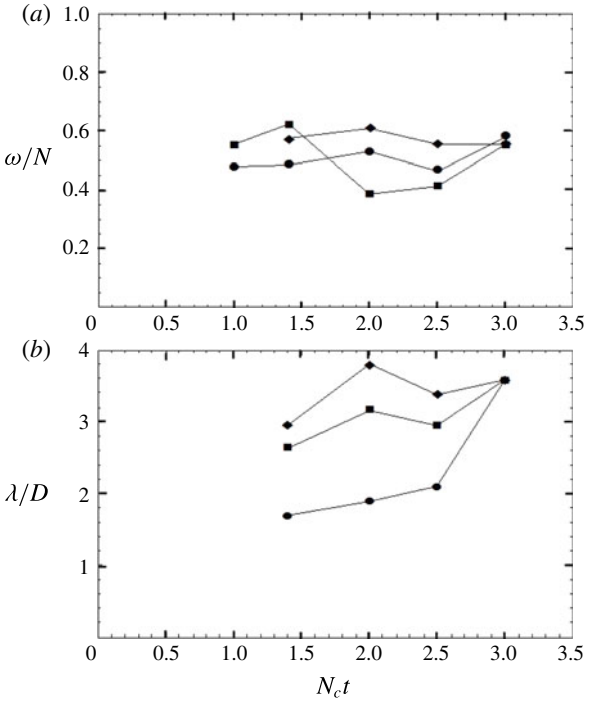

FIGURE 6. Internal wave propagation in the vertical plane, $Fr = 1/\pi$. (*a*) Effective forcing frequency (wave angle according to dispersion relation, (3.2)): ●, first crest; ■, first trough; ◆, second crest. (*b*) Horizontal wavelength: ●, $z/R = 2.11$; ■, $z/R = 2.11$; ◆, $z/R = 3.79$.

Diamessis & Abdilghanie (2011) and Abdilghanie & Diamessis (2013) for turbulent wake-generated IWs of $\lambda/D \simeq 1.5$ for $Fr = 2$ in the range of $N_c t = 1.6$–30. This is expected since the lee wave forcing scale is considerably larger than the characteristic dimension of the wake eddies.

The increase in the spreading angle and increased wavelengths further from the source were explained by Cerasoli (1978) based on an argument of Wu (1969). In effect, as the IWs are generated by a broadband source, the waves with longer wavelengths will have larger phase and group speeds than those with shorter wavelengths, with the result that they will propagate farther from the source and more rapidly propagate off track, resulting in an increasing angle of the rays connecting the crests and troughs.

3.2.4. *IW spreading in the horizontal plane*

Horizontal (x–y plane) spreading of the IW field was investigated by plotting the mean IW amplitudes at specified depths for the seven Nt conditions at $Fr = 1/\pi$ given in table 2. The resulting plots at three depths are shown in figure 7. Connecting the crests and troughs of the evolving waveforms, as illustrated by the dashed lines in figure 7, illustrates the spreading, or local 'opening angle', ϕ, of the IW pattern with time (or downstream distance). Measured values of ϕ for the off-centre wave troughs and crests are shown in figure 8. (The value at $z/D = 1.9$ was computed as a least-squares fit to the off-track distance of each of the individual IW wave crests (40 total) listed in table 2, as a check.) Clearly ϕ increases with height above

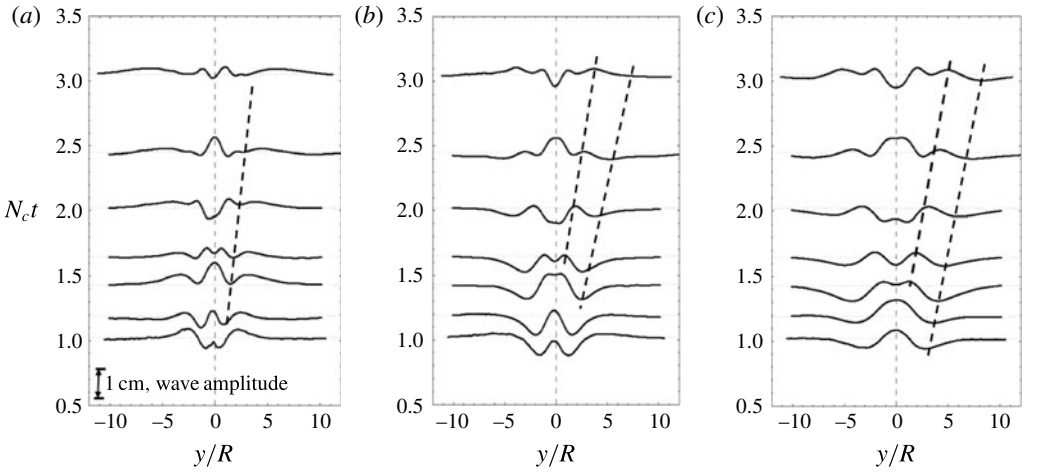

FIGURE 7. Internal wavefield spreading, $Fr = 1/\pi$: (*a*) $z/R = 1.05$; (*b*) $z/R = 2.11$; (*c*) $z/R = 3.16$.

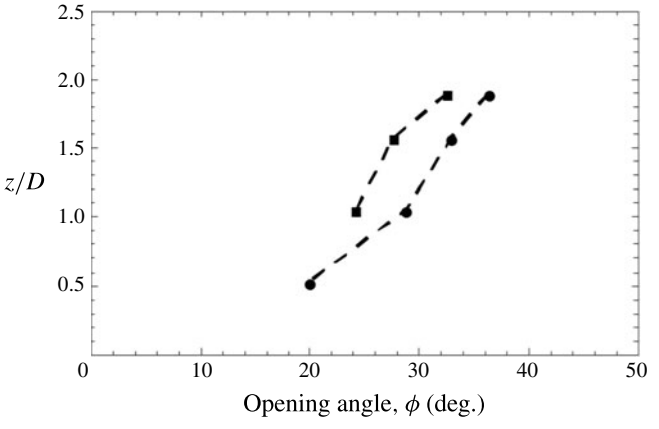

FIGURE 8. Internal wavefield opening angle, $Fr = 1/\pi$: ●, first trough; ■, first crest.

the sphere; this is in accordance with the low-*Fr* analytical model (Vasholz 2011). Here, ϕ increases in an approximately linear manner with distance above the sphere, with outermost trough spreading faster, in agreement with the increased wave speed associated with the longer wavelengths at larger distances from the sphere (discussed in § 3.2.3).

The opening angles computed by Robey (1997) for the mode-1 IWs and by the equation derived by Vasholz (2011) for the lower modes (i.e. modes 1, 2 and 3) are considerably narrower than observed in the present experiments. This difference can be attributed to the fact that, in contrast to the later-time evolution modelled by Robey (1997) and Vasholz (2011), where the opening angles were computed for IW evolution over 15 cycles ($N_c t \leqslant 15$), the present results are confined to the very near field (i.e. three cycles, $N_c t \leqslant 3$) where the broadband IW source is generating a signature that is, from the analytic perspective, the sum of multiple modes that often do not have a clear pattern, as demonstrated by Sharman & Wurtele (1983).

However, the experimental results shown by Robey (1997) show a significantly wider band of IWs at early times at low Fr, extending beyond the central band, which matches the mode-1 calculations. Geometrically scaling ϕ for the broader waves at the lowest speed shown by Robey (1997), which corresponds to $Fr = 0.44$, yields $\phi \approx 32°$. This is in agreement with the present results (figure 8) considering that Robey's measurements are for a pycnocline stratification, in contrast to the uniform stratification of the present experiments.

3.3. *Turbulent wake*

While measurement of the properties of the turbulent wake itself was not the primary objective of the present study, it was possible to use the cross-plane displacement data to determine the wake geometric properties. In general, the turbulent wake contains both wave-like and turbulent-like motions, which are difficult, if not impossible, to clearly separate (Jacobitz, Rogers & Ferziger 2005; Brandt & Schemm 2011; Vasil'ev, Voropaeva & Kurbatskii 2011). As the data in the wake region are aliased as a result of insufficient sampling in the turbulent region, as evident in figure 2, only a determination of the boundaries of the region containing the high-frequency fluctuations could be obtained, providing estimates of the height and width of the turbulent wake region. In general, it can be observed from the present data (e.g. figures 2 and 3) that the turbulent wake region extends to a height of $z/D \approx 0.45$, in agreement with the calculations of Abdilghanie & Diamessis (2013), where the wake extends to $z/D = 0.5$ at comparable Fr and Re.

By trying several methods to delineate the wake, it was found that using a threshold level of the slope of cross-track IW PE density at each probe yielded a reasonably definitive demarcation of the wake region. The IW PE was computed using the square of the IW amplitude, ζ, at each point along the probe traverse as

$$\mathrm{PE} = \tfrac{1}{2}\rho N^2 \zeta^2. \tag{3.3}$$

The evolution of the maximum wake height, H_w, and width, W_w, determined for each run ensemble using this criterion is shown in figure 9 for the wake evolution data at $Fr = 1/\pi$. The error bars represent the standard deviation for the runs in the each ensemble group; for the wake height, the maximum of the standard deviation and the probe spacing interval was used. Although these data encompass a limited down-track range, $x/D = 2.0$–6.1, the overall trends of wake height showing the collapse, due to the onset of buoyancy effects, and subsequent rise and the generally steady growth in wake width are in general agreement with prior results at higher Froude numbers (see e.g. Lin *et al.* (1992*a*) for a towed sphere and Lin & Pao (1979) and Gilreath & Brandt (1985) for self-propelled slender bodies).

Specifically, as shown in figure 9(*a*), the maximum wake height prior to collapse is $H_w/D = 1.1$ and the extent of collapse is $\Delta H_w/D = 0.27$. The wake geometry data at low Fr in Lin *et al.* (1992*a*) show that, within the scatter of the data, the downstream location of the height minimum decreases as the Froude number decreases, with the minimum occurring at $Nt = 1.6$ at $Fr = 1$, with $H_w/D \simeq 1.0$ and $\Delta H_w/D \simeq 0.5$. Comparisons to the present data are not unreasonable considering that the present data are at a considerably lower Froude number. Overall, however, the generally slow growth in H_w/D is in agreement with the essentially constant wake height in the $Nt < 80$ regime described in the self-similar wake evolution diagram in Spedding (2014, figure 3(b)).

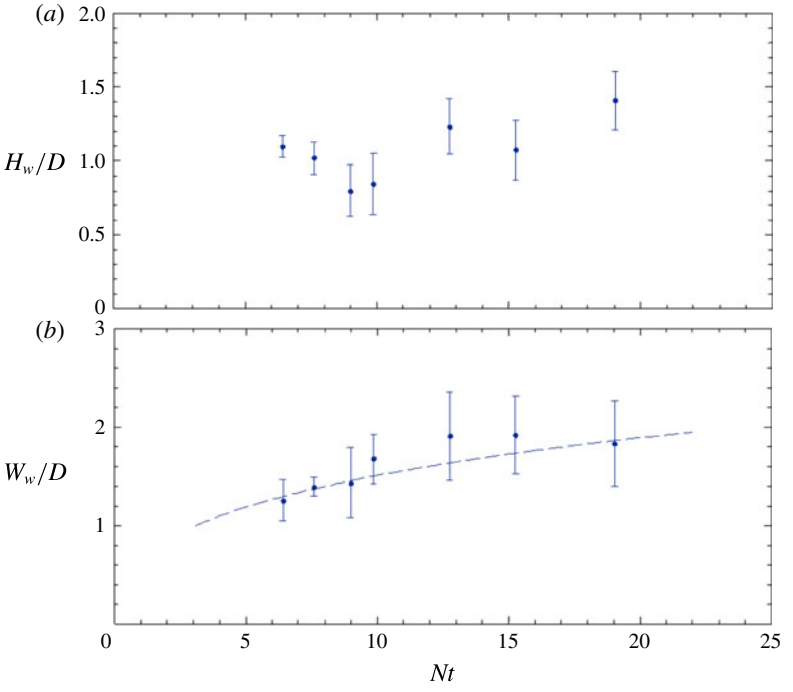

FIGURE 9. (Colour online) Evolution of turbulent wake, $Fr = 1/\pi$: (*a*) wake height; (*b*) wake width (dashed line is $\propto (Nt)^{1/3}$).

The wake width (figure 9*b*) grows as $\sim(Nt)^{1/3}$ in agreement with Lin *et al.* (1992*a*) and Spedding *et al.* (1996*b*), as shown by the dashed curve that is positioned to have $W_w/D = 1.0$ at $x/D = 1.0$ ($Nt = 3.1$). The levelling off of the present data at larger values of Nt may be indicative of the decay of the turbulence within the wake at later times.

3.4. *Internal wave potential energy*

3.4.1. *Variation of IW PE with Froude number*

To characterize the strength of the IW field generated by the towed sphere, the PE per unit down-track distance within the probe rake aperture, PE_A, was computed for each of the individual runs listed in tables 1 and 2. PE_A was computed from the square of the wave amplitude, ζ, along the probe rake cuts, integrated over rake aperture as

$$\mathrm{PE}_A = \iint_{(z,y)} \frac{1}{2}\rho_0 N^2 \zeta^2 \,\mathrm{d}y\,\mathrm{d}z. \tag{3.4}$$

Integration in the cross-track direction was carried out by summation of the displacements at each digitized point obtained as the probe rake traversed the IW field (0.6 cm apart). Vertical integration was performed by assuming that the IW field obtained for each probe is representative of the pattern halfway to the neighbouring probe. As the lower probes (those at $z/D < 5$) traversing the turbulent wake region are not measuring a clearly defined IW field (due to the presence of the turbulent wake discussed in § 3.2), and are aliased due to the sampling rate, the lowest five probes

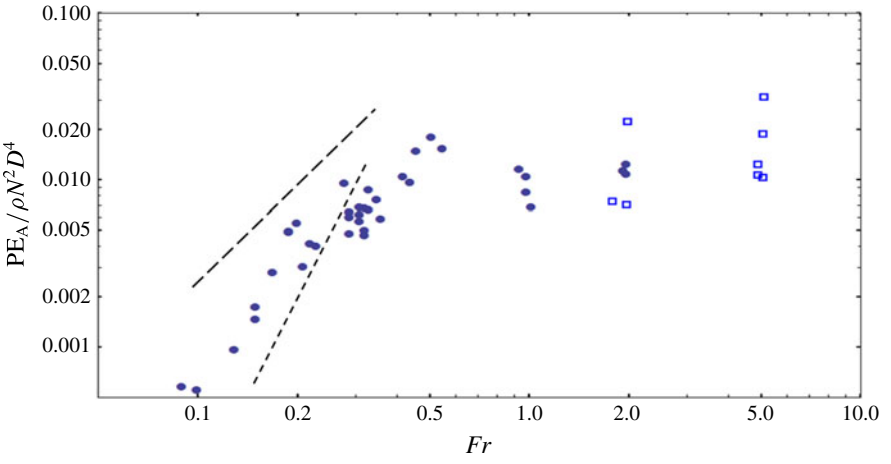

FIGURE 10. (Colour online) Froude-number dependence of IW PE, $Nt = 2\pi$: ●, $N = 1.20$ s^{-1}; □, $N = 0.20$ s^{-1}. Long dashed line is $\propto Fr^2$; short dashed line is (3.6), $\propto Fr^{7/2}$.

were excluded from the calculation of PE_A; i.e. (3.4) is integrated over the range $z/D = 0.47$–1.95. As the probe rake spanned 86 % of the stratified upper region of the water column, PE_A provides a reasonable relative measure of the energy coupled into the IW field (extrapolation to the total PE is discussed in § 3.4.2).

PE_A as a function of Fr computed for each of the individual runs within each group listed in table 1 is shown in figure 10. While the IW traces at low Fr appear qualitatively repeatable (see figures 2 and 3), the variability in PE_A is apparent. This is the result of variability of the forcing by the recirculation zone behind the sphere, and to some degree experimental error. At higher Fr, $Fr \geqslant 1$, the spread in PE_A reflects the inherent variability due to the contributions from the turbulent wake. As discussed in § 2.1, most of the data were obtained with a linear stratification of $N = 1.20$ s^{-1}. To achieve higher values of Fr, the stratification was reduced to $N = 0.20$ s^{-1}, shown by the unfilled points in figure 10 at $Fr \approx 2$ and 5. The general agreement of the PE_A values at $Fr \approx 2$ for both stratifications provides a level of confirmation of the overall approach. Data obtained at a higher tow speed in the weak stratification to achieve $Fr \approx 10$ had substantially larger wake turbulence displacements extending well beyond the designated wake region, $z/D \leqslant 0.45$, prohibiting the use of these data for computing PE_A.

Figure 10 illustrates the existence of several regimes characterizing the coupling between the body-generated lee waves at low Fr and the turbulent wake-generated IWs at larger Fr. In the lee wave regime at low Fr, $Fr \leqslant 0.5$, PE_A increases approximately $\propto Fr^2$, reaches a maximum at $Fr \sim 0.5$, and decreases until $Fr \approx 1$. At this point the turbulent wake becomes the dominant source of IWs and PE_A again increases. These trends resulting from the present comprehensive measurements of the sphere-generated IW field are in general agreement with prior more limited observations that generally considered only the amplitude of a specific constant density level. The observed low-Fr growth rate of $PE_A \propto Fr^2$ agrees with the wave amplitude growth rate $\propto Fr$ observed by Chomaz *et al.* (1993*b*) (note that the PE is proportional to the square of the wave amplitude as seen in (3.4)). This result differs, however, from the amplitude growth rate $\propto Fr^2$ found by Robey (1997), which is most certainly the result of the pycnocline stratification that trapped the internal wavefield. It should

be noted, however, that lee wave displacements produced in different vertical regions are predicted to have different Froude-number dependences (Greenslade 2000; Voisin 2007), so that the comparisons of the present data that are an integrated average over the entire wavefield to the wave amplitudes measured at specific locations by Chomaz *et al.* (1993*b*) and Robey (1997) should be considered as qualitative. The Froude number at which the resonant lee wave coupling maximum occurs agrees with observations of Chomaz *et al.* (1993*b*) and Robey (1997) and with the peak in the sphere drag measured by Lofquist & Purtell (1984), and it is reasonably close to the analytical prediction of $Fr \sim 0.46$ (Vasholz 2002). Further comparisons to lee wave models are presented in § 3.4.3. Finally, the transition between the lee wave and the turbulent wake generation regimes agrees with the $Fr \approx 2$ location noted by Chomaz *et al.* (1991), Hopfinger *et al.* (1991), Lin *et al.* (1993) and Robey (1997). The large run-to-run variation in PE_A at $Fr = 2$ and 5 (and to some degree at $Fr = 1$) is due to the presence of wake turbulence-generated IWs, as further discussed in the following section.

3.4.2. *Total PE in the IW field*

Using the measurements of PE_A, it is possible to estimate the fraction of the total input energy that is manifest in the internal wavefield. To obtain this estimate, it is assumed that the region of the water column covered by the probes (86 % of the upper half) is representative of the whole water column, so that increasing PE_A by a factor of 1.16 and multiplying by 2 (to account for the bottom half of the IW field) will yield the total IW PE, PE_T, exclusive of that present within the turbulent wake region. Because of these approximations, estimates of the total IW PE should be considered somewhat more qualitative than quantitative.

For a towed body, the total energy input per unit down-track distance to the turbulent wake and the internal wavefield is equal to the drag force on the sphere, $\mathscr{D} = (\rho C_D U^2 A)/2$, where C_D is the drag coefficient and A is the sphere cross-sectional area. For spheres in a stratified flow, detailed measurements of $\mathscr{D}$ in terms of changes in C_D as a function of Fr were made by Lofquist & Purtell (1984). It should also be noted that the Reynolds-number regime considered is lower than that where the drag crisis exists ($Re < 5 \times 10^4$ for roughened spheres), so that sphere roughness does not affect its drag due to the fact that the boundary layer separates while it is still laminar with the roughness elements embedded within the boundary layer (Hoerner 1958; Achenbach 1974). These values are used to compute $\mathscr{D}$ in figure 11(*a*), which shows the ratio of PE_T to the measured sphere drag as a function of Fr. These values were obtained by averaging the values of PE_A computed from each of the individual runs at each condition listed in table 1, grouped into local Fr bins in order to provide a more accurate estimate. The error bars show the standard error of the mean for each bin. Here, PE_T represents an estimate of the total IW PE resulting from both the body and turbulent wake sources.

The most striking result shown is the strong coupling of the input energy to the IW field in the regime $0.2 \lesssim Fr \lesssim 0.6$, where $\mathrm{PE}_T/\mathscr{D}$ ranges from 40 % to 70 %. The balance of the total energy input is manifest as the kinetic energy (KE) associated with the IWs and the PE and KE in the turbulent wake. This strong coupling results from the balance between the larger IW PE at higher Fr (figure 10) and the increased drag at lower Fr (Lofquist & Purtell 1984) and can be explained in terms of the inherent environmental resonance of the stratified flow field (Vasholz 2002). In this low-Fr regime, where PE_A increases considerably ($\propto Fr^2$) towards the resonance peak, the fraction of the total input energy, $\mathrm{PE}_T/\mathscr{D}$, going into the IW field, increasing at

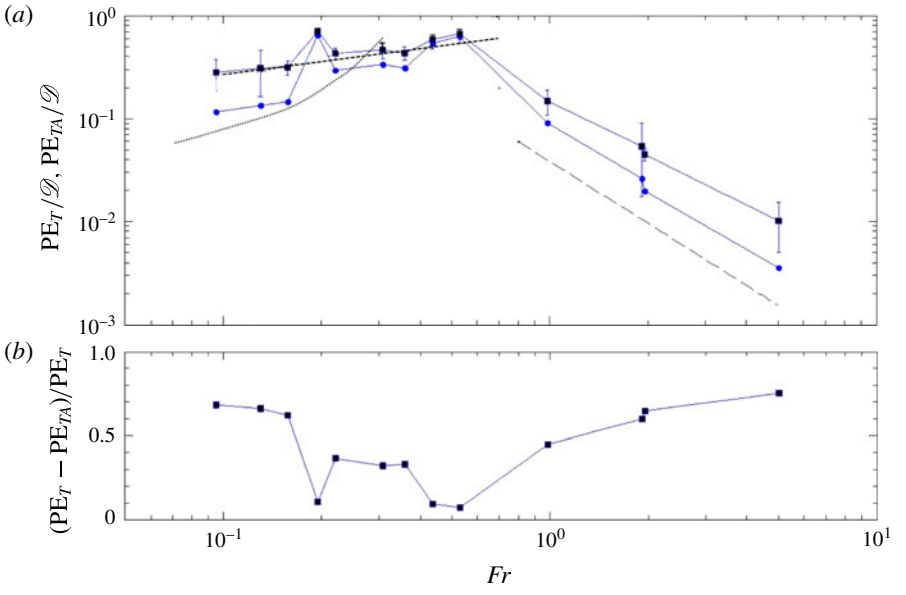

FIGURE 11. (Colour online) Total wavefield PE, $Nt = 2\pi$. (*a*) PE as fraction of energy input: ■, PE_T; ●, PE_{TA}. Short dashed line is $\propto Fr^{1/2}$; long dashed line is $\propto Fr^{-2}$, dotted line is (3.8). (*b*) Random wake forcing contribution to total PE.

only a moderate rate, is approximately $\propto Fr^{1/2}$, as shown by the short dashed line in figure 11(*a*).

For values of $Fr \gtrsim 1$, where the turbulent wake source becomes dominant, $\mathrm{PE}_T/\mathscr{D}$ decreases with Fr by almost two orders of magnitude by $Fr \sim 5$, despite the fact that the turbulent wake-generated IW contribution increases with Fr when $Fr \gtrsim 1$ (figure 10), indicating a larger fraction of energy going into wake turbulence itself. This is qualitatively in agreement with the numerical simulations of turbulent wake-generated IW of Abdilghanie & Diamessis (2013), which show a decrease in wake momentum lost, presumably to the IW field, as Fr increases using simulations at $Fr = 2$, 8 and 32.

Alternatively, computing PE from the mean of the measured wavefield amplitudes at each test condition, designated PE_{TA}, results in a measure of the repeatable component of the IW field, as shown in figure 11(*a*). In the strong coupling region, $0.2 \lesssim Fr \lesssim 0.6$, the non-repeatable component of the PE_T is small: the difference, $(\mathrm{PE}_T - \mathrm{PE}_{TA})/\mathrm{PE}_T$, is shown in figure 11(*b*). The increase in $(\mathrm{PE}_T - \mathrm{PE}_{TA})/\mathrm{PE}_T$ at low values of Fr is probably the result of variations in PE_T due to the fact that at these low Fr values the $\mathrm{PE}_T/\mathscr{D}$ and $\mathrm{PE}_{TA}/\mathscr{D}$ are ratios of two small numbers (cf. figure 10). While the integrated PE estimates shown in figures 11 and 12 do not show any direct evidence of depth-dependent resonances at discrete values of Fr_H (as discussed in § 1.3), the finite tank depth would be a contributing factor to the observed IW PE levels. In the large-Fr region, $Fr \gtrsim 1$, $\mathrm{PE}_{TA}/\mathscr{D}$ decreases $\propto Fr^{-2}$ (shown as the long dashed line), indicative of the lessening influence of the lee wave forcing mechanism, while $\mathrm{PE}_T/\mathscr{D}$ decreases at a slower rate, approximately $\propto Fr^{-3/2}$, indicating the increased IW forcing by the turbulent wake, the fraction of which is shown in figure 11(*b*).

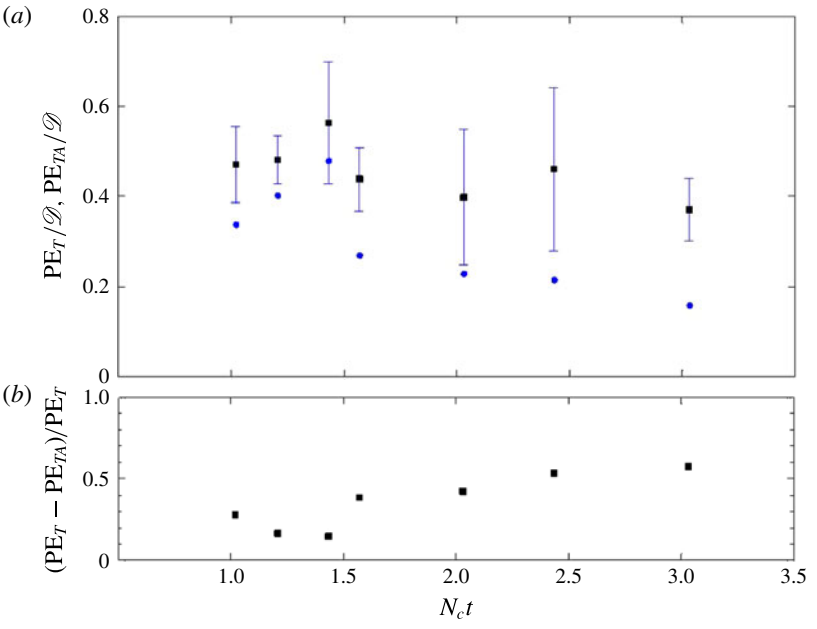

FIGURE 12. (Colour online) Temporal evolution of wavefield total PE, $Fr = 1/\pi$. (*a*) PE as fraction of energy input: ■, PE_T; ●, PE_{TA}. (*b*) Random wake forcing contribution to total PE.

3.4.3. *Comparisons to lee wave models*

Bell (1975) developed a two-dimensional linear solution for lee waves generated by a topographic (body) source in an oscillating flow. For a particular topographic shape, a solution for the dimensionless power, $\overline{\mathscr{P}}/(\pi/4)\rho_0 U_0^2 N D^2$ (rate of energy), being fed to the internal wavefield at zero oscillation frequency (steady flow) in the low-Fr limit ($Fr \to 0$) is a constant. When converted from power to energy per unit distance using the average over one BV cycle and then to the dimensionless form used herein results in energy/$(\rho N^2 D^4) \sim (\pi^2/4)Fr^2$, which agrees with the experimentally determined behaviour at low Fr shown in figure 10. The actual values, however, are more than an order of magnitude larger than the present experimental values of IW PE. Owing to the differences between Bell's model and the present experiment (i.e. Bell (1975) considers a two-dimensional continuous reinforcing flow over a specific mountain shape (witch of Agnesi) as compared to the present transient forcing situation), only qualitative agreement would be expected. Thus the agreement of Bell's result with the apparent trend in figure 10 is somewhat fortuitous.

As the pressure drag on the sphere results from the generation of IWs and the separation of the boundary layer from the sphere surface, modelling of the sphere drag has been divided into two components. Semi-empirical relationships for the Froude number dependence of lee wave drag have been derived by Greenslade (2000), Voisin (2007) and Dalziel *et al.* (2011) for both the wave and wake contributions. For the low-Fr limit, $Fr \to 0$, the corresponding drag coefficients are $C_D^{wave} \propto Fr^{3/2}$ and $C_D^{wake} \propto Fr^{1/2}$. For comparison to the present IW PE results, consider the wave component given by

$$C_D^{wave} = 2^{3/2} B Fr^{3/2}, \tag{3.5}$$

where B is based on the empirical fit to the experimental data or the analytically derived value of $B=(32\sqrt{2})/15\pi\simeq 0.960$ (Voisin 2007) and the Froude number based on the sphere radius is converted to the present diameter-based Froude number. Thus the drag due to the induced waves $\mathscr{D}^{wave}=(\rho C_D^{wave}U^2(\pi D^2/4))/2$, converted to the present scaling, is given by

$$\frac{\mathscr{D}^{wave}}{\rho N^2 D^4}=1.22\frac{\pi}{8}BFr^{7/2}, \tag{3.6}$$

where the factor 1.22 results from the finite aperture of the probe rake as discussed in § 3.4.2.

As $\mathscr{D}^{wave}$ is equivalent to the energy per unit downstream input into the IW field by lee wave forcing, this relation is shown on figure 10 as a short dashed line. The slope of this theoretical estimate matches reasonably well with the experimental data for $Fr\lesssim 0.3$; however, the magnitude given by (3.5) is slightly low. A value of the constant $B\approx 2.5$ would fit the data. This difference could be the result of effects of the finite depth of the tank.

The total IW PE at low Fr shown in figure 11 can be compared to (3.5) by computing the wave component of the lee wave drag as a fraction of the total lee wave drag as $\mathscr{D}^{wave}/\mathscr{D}=C_D^{wave}/(C_D^{wave}+C_D^{wake})$, with

$$C_D^{wake}=2^{1/2}CFr^{1/2}(1+\tfrac{5}{2}Fr), \tag{3.7}$$

where C is a fit to the experimental drag measurement data (Voisin 2007), yielding

$$\frac{\mathscr{D}^{wave}}{\mathscr{D}}=\left[\frac{1}{2}\frac{C}{B}Fr^{-1}+\left(1-\frac{5}{4}\frac{C}{B}\right)\right]^{-1}, \tag{3.8}$$

approximately $\propto Fr$. Using the analytic value for B and the drag data fitted value of $C\approx 3.33$ (Voisin 2007), (3.8) is shown as a dotted line on figure 11, where it should be compared to $\mathrm{PE}_{TA}/\mathscr{D}$, as it represents the steady lee wave component. The agreement is quite reasonable.

Model comparison at high Froude numbers is rather problematical, as the lee wave models are inviscid and thus in the high-Fr limit do not account for the turbulence-generated IWs, which tend to dominate at $Fr\gtrsim 0.5$. In the limit as $Fr\to\infty$, $C_D^{wave}\propto Fr^{-4}$ and $C_D^{wake}\propto C_D(\infty)$, where $C_D(\infty)$ is the drag coefficient for the unstratified limit (Gorodtsov & Teodorovich 1982), taken as 0.51 based on the experimental studies (Voisin 2007). This results in $\mathscr{D}^{wave}/(\rho N^2D^4)\propto Fr^{-2}$ and $\mathscr{D}^{wave}/\mathscr{D}\propto Fr^{-4}$, which as expected have a significantly greater falloff than the experimental data (figures 10 and 11) due to the additional presence of IWs resulting from the random wake eddies in the experimental data.

3.4.4. *Temporal evolution of total IW PE*

It should be noted that these PE data, figures 10 and 11, represent the near-wake regime, at one BV period ($N_ct=1$), so that the physical fluid displacement generating the IWs is still occurring (as also evident in the early-time evolution of the IW shown in Gilreath & Brandt (1985)), causing a large contribution to the IW PE and less to the IW KE as the wavefield has not had time to equilibrate. Figure 12(*a*) shows the temporal evolution of both the PE_T and the repeatable component PE_{TA} as functions of downstream evolution for three BV periods for the test series listed in table 2. Each

point shown represents the mean of the repeated runs at each value of $N_c t$, with the error bars representing the standard error of the mean for each value of $N_c t$ measured. The $\sim 2/3$ decrease in $\mathrm{PE}_{TA}/\mathscr{D}$ with $N_c t$ at $N_c t = 3.03$ from its maximum at $N_c t = 1.45$ is indicative of the lessening influence of the lee wave generation mechanism and the trend towards IW equipartition. The increase in the non-repeatable component due to the increasing contribution of the turbulent wake IW source is evidenced by the decrease in $\mathrm{PE}_T/\mathscr{D}$ (by $\sim 1/3$ at $N_c t = 3.03$ from its maximum at $N_c t = 1.45$) and the increased difference in $(\mathrm{PE}_T - \mathrm{PE}_{TA})/\mathrm{PE}_T$, shown in figure 12(*b*).

4. Summary and discussion

An extensive experimental investigation of the near-field internal wavefield generated by a towed sphere at low Froude number in a uniformly stratified fluid has been performed. The results have provided a characterization of the wavefield patterns. Vertical spreading angles in the near field of $\theta \simeq 55°$–$65°$ were measured, which are considerably shallower than the angles characteristic of higher-Fr turbulent IW sources. This is due to the inherently lower frequencies associated with the low-Fr body generation mechanism. Wavefield spreading in the horizontal was found to increase with distance above the sphere, ranging over $\phi = 20°$–$35°$ for $z/D = 0.5$–1.9. The increase in ϕ with distance is in agreement with the low-Fr analytical model of Vasholz (2011). However, these values differ considerably from the far-field patterns evident in the experiments of Robey (1997) and point-source far-field models (e.g. Keller & Munk 1970). This difference is due to the presence of significant contributions from higher IW modes in the near field. The early-time low-Fr experimental results shown by Robey (1997) show a significantly wider IW band that extends beyond the central band, which matches his mode-1 calculations and those of Vasholz (2011).

Quantitative measurements of the IW PE, as a function of Froude number and distance behind the body, as well as the relative contributions of the IW generated by body forcing, rather than those generated by the turbulent wake, have been determined, extending the previous measurements of Gilreath & Brandt (1985) and Robey (1997). Specifically, it was found that, at one BV period, the IW PE reached a maximum at $Fr \sim 0.5$ (figure 10), in agreement with the peak IW amplitude at $Fr = 0.5$–0.7 measured from particle streak images by Chomaz *et al.* (1993*b*) and in reasonable agreement with the peak amplitude at $Fr = 0.7$–0.8 measured from an individual probe in a pycnocline layer (Robey 1997). It was found that up to 70 % of the input energy is converted to IWs at low Fr (figure 11). This peak in IW PE occurs in the regime $0.2 \lesssim Fr \lesssim 0.6$, corresponding to analytical prediction of a lee wave coupling resonance at $Fr \sim 0.46$ (Vasholz 2002) and explaining the increase in drag at low Fr observed by Lofquist & Purtell (1984). At this early time, the effect of the body (lee wave) forcing is to displace the fluid, resulting in an imbalance in the PE/KE ratio that ameliorates as time progresses (figure 12). Although the IW KE was not measured, it is not unreasonable to conclude that, in this low-Fr regime, virtually all of the input energy is manifest as IWs. At larger values, $Fr \gtrsim 1$, when the turbulent wake source contribution becomes significant, the energy input to the IW field increases considerably; however, the IW energy becomes a decreasing fraction of the input energy, the balance increasingly going into the turbulent wake.

Finally, it should be noted that at high Fr (i.e. $Fr \gtrsim 1$), where turbulent wake forcing becomes dominant, the IW field above the wake region has a coherent structure, as illustrated in figure 4(*c*,*d*) (albeit with asymmetries present at higher Fr due to

the insufficient number of ensemble samples), similar to that present at lower-Fr conditions (as shown in figures 2, 3 and 4*a*,*b*). This is also observed in the case of a self-propelled slender body at $Fr = 5.3$ as shown in Gilreath & Brandt (1985), and for IW generated by a continuous turbulent source as in Dohan & Sutherland (2005).

Acknowledgements

The support of J. E. Hopkins in the conduct of the experiments, the effort of K. R. Shipley for review and editing, and the scientific collaboration with C. E. Schemm and H. E. Gilreath are greatly appreciated. This effort was supported by the Office of Naval Research Turbulence and Stratified Wakes Program, L. P. Purtell and R. D. Joslin, programme managers; their ongoing support is highly appreciated. The insightful comments of the anonymous reviewers resulted in significant improvements to the manuscript.

REFERENCES

ABDILGHANIE, A. M. & DIAMESSIS, P. J. 2013 The internal gravity wave field emitted by a stably stratified turbulent wake. *J. Fluid Mech.* **720**, 104–139.

ACHENBACH, E. 1974 The effects of surface roughness and tunnel blockage on the flow past spheres. *J. Fluid Mech.* **65**, 113–125.

BAINES, P. 1995 *Topographic Effects in Stratified Flows*. Cambridge University Press.

BELL, T. H. 1975 Lee waves in stratified flows with simple harmonic time dependence. *J. Fluid Mech.* **67**, 705–722.

BONNETON, P., CHOMAZ, J. M. & HOPFINGER, E. J. 1993 Internal waves produced by the turbulent wake of a sphere moving horizontally in a stratified fluid. *J. Fluid Mech.* **254**, 23–40.

BONNETON, P., CHOMAZ, J. M., HOPFINGER, E. J. & PERRIER, M. 1996 The structure of the turbulent wake and the random internal wave field generated by a moving sphere in a stratified fluid. *Dyn. Atmos. Oceans* **23**, 299–308.

BONNIER, M. & EIFF, O. 2002 On experimental investigation of the collapse of a turbulent wake in a stably stratified fluid. *Phys. Fluids* **14**, 791–801.

BRANDT, A. 1999 Evolution of vortices generated by the collapse of a stratified, turbulent wake. In *IUGG-99, XXII General Assembly, 19–30 July 1999, presentation, Birmingham, UK. IUGG*.

BRANDT, A. & SCHEMM, C. E. 2011 Small-scale structure in the near field of a stratified wake. In *Proceedings of the 7th International Symposium on Stratified Flows, Rome, Italy, 22–26 August 2011*.

BRUCKER, K. A. & SARKAR, S. 2010 A comparative study of self-propelled and towed wakes in a stratified fluid. *J. Fluid Mech.* **652**, 373–404.

CASTRO, I. P., SNYDER, W. H. & BAINES, P. G. 1990 Obstacle drag in stratified flow. *Proc. R. Soc. Lond.* A **429**, 119–140.

CERASOLI, C. P. 1978 Experiments on buoyant-parcel motion and the generation of internal waves. *J. Fluid Mech.* **86**, 247–271.

CHANG, Y., ZHAO, F., ZHANG, J., HONG, F.-W., LI, P. & YUN, J. 2006 Numerical simulation of internal waves excited by a submarine moving in the two-layer stratified fluid. *J. Hydrodyn.* **18** (3), 330–336; Supplement 1.

CHERNYSHENKO, S. I. & CASTRO, I. P. 1996 High-Reynolds-number weakly stratified flow past an obstacle. *J. Fluid Mech.* **317**, 155–178.

CHOMAZ, J. M., BONNETON, P., BUTET, A. & HOPFINGER, E. J. 1993*a* Vertical diffusion in the far wake of a sphere moving in a stratified fluid. *Phys. Fluids* A **5**, 2799–2806.

CHOMAZ, J. M., BONNETON, P., BUTET, A., HOPFINGER, E. J. & PERRIER, M. 1991 Gravity wave patterns in the wake of a sphere in a stratified fluid. In *Turbulence and Coherent Structures* (ed. O. Metais & M. Lesieur), pp. 489–503. Kluwer Academic.

CHOMAZ, J. M., BONNETON, P., BUTET, A. & PERRIER, M. 1992 Froude number dependence of the flow separation line on a sphere towed in a stratified fluid. *Phys. Fluids* A **2**, 254–258.

CHOMAZ, J. M., BONNETON, P. & HOPFINGER, E. J. 1993*b* The structure of the near wake of a sphere moving horizontally in a stratified fluid. *J. Fluid Mech.* **254**, 1–21.

DALZIEL, S. B., PATTERSON, M. D., CAULFIED, C. P. & LE BRUN, S. 2011 The structure of low-Froude-number lee waves over an isolated obstacle. *J. Fluid Mech.* **689**, 3–31.

DESILVA, I. P. D. & FERNANDO, H. J. S. 1998 Experiments on collapsing turbulent regions in stratified fluids. *J. Fluid Mech.* **358**, 29–60.

DIAMESSIS, P. J. & ABDILGHANIE, A. M. 2011 The internal wave field radiated by a stably stratified turbulent wake. In *Proceedings of the 7th International Symposium on Stratified Flows, Rome, Italy, 22–26 August 2011*.

DIAMESSIS, P. J., GURKA, R. & LIBERZON, A. 2010 Spatial characterization of vortical structures and internal waves in a stratified turbulent wake using proper orthogonal decomposition. *Phys. Fluids* **22**, 086601.

DIAMESSIS, P. J., SPEDDING, G. R. & DOMARADZKI, J. A. 2011 Similarity scaling and vorticity structure in high-Reynolds-number stably stratified turbulent wakes. *J. Fluid Mech.* **671**, 52–95.

DOHAN, K. & SUTHERLAND, B. R. 2005 Numerical and laboratory generation of internal waves from turbulence. *Dyn. Atmos. Oceans* **40**, 43–56.

DUPONT, P., KADRI, Y. & CHOMAZ, J. M. 2001 Internal waves generated by the wake of Gaussian hills. *Phys. Fluids* **13**, 3223–3233.

DUPONT, P. & VOISIN, B. 1996 Internal waves generated by a translating and oscillating sphere. *Dyn. Atmos. Oceans* **23**, 289–298.

GILREATH, H. E. & BRANDT, A. 1985 Experiments on the generation of internal waves in a stratified fluid. *AIAA J.* **23**, 693–700.

GORODTSOV, V. A. & TEODOROVICH, E. V. 1982 Study of internal waves in the case of rapid horizontal motion of cylinders and spheres. *Fluid Dyn.* **17**, 893–898; [Transl. from *Izv. Akad. Nauk SSSR Mekh. Zhidk. Gaza* **17** (6), 94–100].

GOURLAY, M. J., ARENDT, S. C., FRITTS, D. C. & WERNE, J. 2001 Numerical modeling of initially turbulent wakes with net momentum. *Phys. Fluids* **13** (12), 3783–3802.

GREENSLADE, M. D. 2000 Drag on a sphere moving horizontally in a stratified fluid. *J. Fluid Mech.* **418**, 339–350.

HOERNER, S. F. 1958 *Fluid-Dynamic Drag*. Published by the author.

HOPFINGER, E. J., FLOR, J.-B., CHOMAZ, J.-M. & BONNETON, P. 1991 Internal waves generated by a moving sphere and its wake in a stratified fluid. *Exp. Fluids* **11**, 255–261.

JACOBITZ, F. G., ROGERS, M. M. & FERZIGER, J. H. 2005 Waves in stably stratified turbulent flow. *J. Turbul.* **6** (N32), 1–12.

KELLER, J. B. & MUNK, W. H. 1970 Internal wave wakes of a body moving in a stratified fluid. *Phys. Fluids* **13**, 1425–1431.

LELONG, M.-P. & RILEY, J. J. 1991 Internal wave–vortical mode interactions in strongly stratified flows. *J. Fluid Mech.* **232**, 1–19.

LIGHTHILL, M. J. 1955 *Waves in Fluids*. Cambridge University Press.

LIGHTHILL, M. J. 1996 Internal waves and related initial-value problems. *Dyn. Atmos. Oceans* **23**, 3–17.

LIN, J.-T. & PAO, Y.-H. 1979 Wakes in stratified fluids. *Annu. Rev. Fluid Mech.* **11**, 317–338.

LIN, Q., BOYER, D. L. & FERNANDO, H. J. S. 1992*a* Turbulent wakes of linearly stratified flow past a sphere. *Phys. Fluids* A **4**, 1687–1696.

LIN, Q., BOYER, D. L. & FERNANDO, H. J. S. 1993 Internal waves generated by the turbulent wake of a sphere. *Exp. Fluids* **15**, 147–154.

LIN, Q., BOYER, D. L. & FERNANDO, H. J. S. 1994 The vortex shedding of a streamwise-oscillating sphere translating through a linearly stratified fluid. *Phys. Fluids* A **6**, 239–252.

LIN, Q., LINDBERG, W. R., BOYER, D. L. & FERNANDO, H. J. S. 1992*b* Stratified flow past a sphere. *J. Fluid Mech.* **240**, 315–354.

LOFQUIST, K. E. B. & PURTELL, L. P. 1984 Drag on a sphere moving horizontally through a stratified liquid. *J. Fluid Mech.* **148**, 271–284.

LONG, R. R. 1972 Finite amplitude disturbances in the flow of inviscid rotating and stratified fluids over obstacles. *Annu. Rev. Fluid Mech.* **4**, 69–92.

MENG, J. C. S. & ROTTMAN, J. W. 1987 Linear internal waves generated by density and velocity perturbations in a linearly stratified fluid. *J. Fluid Mech.* **186**, 419–444.

MOWBRAY, D. E. & RARITY, B. S. H. 1967 A theoretical and experimental investigation of the phase configuration of internal waves of small amplitude in a density stratified liquid. *J. Fluid Mech.* **28**, 1–16.

RILEY, J. J., LELONG, M. P. G. & SLINN, D. N. 1991 Organized structures in strongly stratified flows. In *Turbulence and Coherent Structures* (ed. O. Metais & M. Lesieur), pp. 413–428. Kluwer Academic.

ROBEY, H. F. 1997 The generation of internal waves by a towed sphere and its wake in a thermocline. *Phys. Fluids* A **9**, 3353–3367.

ROTTMAN, J. W., BROUTMAN, D., SPEDDING, G. & DIAMESSIS, P. 2006 A model for the internal wavefield produced by a submarine and its wake in the littoral ocean. In *Proceedings of the 26th Symposium on Naval Hydrodynamics, 17–22 September 2006, Rome, Italy*.

SCASE, M. M. & DALZIEL, S. B. 2004 Internal wave fields and drag generated by a translating body in a stratified fluid. *J. Fluid Mech.* **498**, 289–313.

SCASE, M. M. & DALZIEL, S. B. 2006 Internal wave fields generated by a translating body in a stratified fluid: an experimental comparison. *J. Fluid Mech.* **564**, 305–331.

SCHLICHTING, H. 1968 *Boundary-Layer Theory*, 6th edn. McGraw-Hill.

SHARMAN, R. D. & WURTELE, M. D. 1983 Ship waves and lee waves. *J. Atmos. Sci.* **40**, 396–427.

SPEDDING, G. R. 1997 The evolution of initially-turbulent bluff-body wakes at high internal Froude number. *J. Fluid Mech.* **337**, 283–301.

SPEDDING, G. R. 2014 Wake signature detection. *Annu. Rev. Fluid Mech.* **46**, 273–302.

SPEDDING, G. R., BROWAND, G. K. & FINCHAM, A. M. 1996*a* The long-time evolution of the initially turbulent wake of a sphere in a stable stratification. *Dyn. Atmos. Oceans* **23**, 172–182.

SPEDDING, G. R., BROWAND, G. K. & FINCHAM, A. M. 1996*b* Turbulence, similarity scaling and vortex geometry in the wake of a towed sphere in a stably stratified fluid. *J. Fluid Mech.* **314**, 53–103.

STUROVA, I. V. 1978 Internal waves generated by local disturbances in a linearly stratified liquid of finite depth. *J. Appl. Mech. Tech. Phys.* **19** (3), 330–336.

STUROVA, I. V. 1980 Internal waves generated in an exponentially stratified fluid by an arbitrarily moving source. *Fluid Dyn.* **15** (3), 378–383.

VAN DYKE, M. 1982 *An Album of Fluid Motion*. Parabolic.

VASHOLZ, D. P. 2002 Low Froude number potential energy resonances in uniform stratification. *Phys. Fluids* **14**, 458–461.

VASHOLZ, D. P. 2011 Stratified wakes, the high Froude number approximation, and potential flow. *Theor. Comput. Fluid Dyn.* **25**, 357–379.

VASIL'EV, O. F., VOROPAEVA, O. F. & KURBATSKII, A. F. 2011 Turbulent mixing in stably stratified flows of the environment: the current state of the problem. *Izv. Atmos. Ocean. Phys.* **47** (3), 265–280.

VOISIN, B. 1994 Internal wave generation in uniformly stratified fluids. Part 2. Moving point sources. *J. Fluid Mech.* **261**, 333–374.

VOISIN, B. 1995 Internal wave generation by turbulent wakes. In *Mixing in Geophysical Flows* (ed. O. Metais & M. Lesieur), pp. 291–301. CIMME.

VOISIN, B. 2007 Lee waves from a sphere in a stratified flow. *J. Fluid Mech.* **574**, 273–315.

VOSPER, S. B., CASTRO, I. P., SNYDER, W. H. & MOBBS, S. D. 1999 Experimental studies of strongly stratified flow past three-dimensional orography. *J. Fluid Mech.* **390**, 223–249.

WILLIAMSON, C. H. K. 1996 Three-dimensional wake transition. *J. Fluid Mech.* **328**, 345–407.

WU, J. 1969 Mixed region collapse with internal wave generation in a density-stratified medium. *J. Fluid Mech.* **35**, 531–544.